Journal of Imaging Science and Technology® 63(6): 060409-1–060409-11, 2019.

The Impact of Radial Distortions in VR Headsets on Perceived Surface Slant

Jonathan Tong
Centre for Vision Research, York University, Toronto, Ontario, 4700 Keele St., M3J 1P3, Canada
Department of Psychology, York University, Toronto, Ontario, 4700 Keele St., M3J 1P3, Canada
E-mail: tongj86@yorku.ca

Robert S. Allison▲
Centre for Vision Research, York University, Toronto, Ontario, 4700 Keele St., M3J 1P3, Canada
Department of Electrical Engineering and Computer Science, York University, Toronto, Ontario, 4700 Keele St., M3J 1P3, Canada

Laurie M. Wilcox▲
Centre for Vision Research, York University, Toronto, Ontario, 4700 Keele St., M3J 1P3, Canada
Department of Psychology, York University, Toronto, Ontario, 4700 Keele St., M3J 1P3, Canada

Abstract. *Modern virtual reality (VR) headsets use lenses that distort the visual field, typically with distortion increasing with eccentricity. While content is pre-warped to counter this radial distortion, residual image distortions remain. Here we examine the extent to which such residual distortion impacts the perception of surface slant. In Experiment 1, we presented slanted surfaces in a head-mounted display and observers estimated the local surface slant at different locations. In Experiments 2 (slant estimation) and 3 (slant discrimination), we presented stimuli on a mirror stereoscope, which allowed us to more precisely control viewing and distortion parameters. Taken together, our results show that radial distortion has significant impact on perceived surface attitude, even following correction. Of the distortion levels we tested, 5% distortion results in significantly underestimated and less precise slant estimates relative to distortion-free surfaces. In contrast, Experiment 3 reveals that a level of 1% distortion is insufficient to produce significant changes in slant perception. Our results highlight the importance of adequately modeling and correcting lens distortion to improve VR user experience.* © *2019 Society for Imaging Science and Technology.*
[DOI: 10.2352/J.ImagingSci.Technol.2019.63.6.060409]

1. BACKGROUND

Modern virtual reality (VR) head-mounted displays (HMDs) typically rely on near-eye optics to focus and place images at a fixed optical distance from the viewer [1]. Although crucial for focusing the image and enhancing the immersive quality of VR, optical lenses also introduce undesired distortions in the visual field: magnification is non-uniform and varies with eccentricity from the optical axis [2]. To counteract this radial distortion, developers can transform images with an inverse distortion based on a model of the optical properties of the lenses [3–6]. The most widely used models assume symmetric distortion in which the radial displacement of image features, due to magnification, is an odd-order polynomial function of radial eccentricity (see Eq. (1)). The optics of typical HMDs have increasing magnification away from the optical axis, which produces a pincushion distortion (see Figure 1). The inverse or 'barrel' distortion applied to counter the lens optics introduces decreasing magnification away from the optical axis (see Fig. 1). Ideally, these two distortions would cancel one another, resulting in an undistorted image. However, due to approximations in the modeling of optical properties, manufacturing tolerances and observer anatomical variability, residual distortions are unavoidable.

Little empirical attention has been paid to whether these residual distortions, or even uncorrected levels of distortion, result in measurable perceptual consequences that could impact viewer experience. A study by Kuhl et al. [7] found no significant impact of uncorrected pincushion distortion, in an HMD, on distance judgments estimated through blind walking in a virtual environment. They measured the level of required predistortion correction in their headset (NVIS nVisor SX) to be approximately 10%, but this will vary considerably across consumer HMDs. Unlike the HMD used by Kuhl et al. [7], many of the leading modern-day devices automatically correct for lens distortion in their device drivers. For example, a leading modern-day VR headset, the Oculus Rift, predistorts images by ≈20% to correct for lens distortion (maximum inward radial shift of pixels along the image diagonal). However, some of the more affordable modern HMDs, which use smartphones as displays (e.g. Google Cardboard and Google Daydream™), do not automatically correct for lens distortion or require distortion parameters to be determined and entered by users. Here we assess the effects of radial lens distortion in one such

▲ IS&T Members.

Received July 15, 2019; accepted for publication Oct. 14, 2019; published online Dec. 19, 2019. Associate Editor: N. Tsumura.

1062-3701/2019/63(6)/060409/11/$25.00

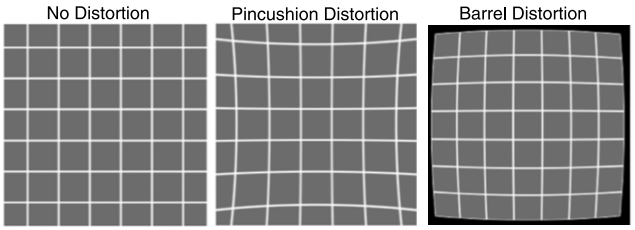

Figure 1. Different types of lens distortion (≈5%) applied to a grid for illustration.

device, the Google Daydream View (v2.0), on local surface slant perception. In addition to radial distortions, the optical properties in HMDs may potentially produce chromatic aberration (independent warping of each color channel), lens glare or even defocus blurring. Here, we specifically focus on the issue of geometric distortion in stereoscopically presented images, while controlling for other factors. Since geometric distortion has varying affects across the visual field, we chose to study its impact on a property derived from disparity and texture gradients spanning the visual field (i.e. surface slant) rather than a strictly local property (e.g. absolute depth). Further motivation for studying the perception of slant is its importance in precise interaction with surfaces in virtual environments (i.e. placement of objects on to surfaces or walking on uneven terrain).

1.1 *Predicted Effects of Distortion on Depth Cues to Slant*

The perceived slant of a surface can be determined by binocular disparity gradients and by monocular texture properties [8–10]. Binocular disparity refers to the positional offset between corresponding points in images projected to the left and right eyes; points with larger binocular disparity appear more distant from the screen plane (plane of fixation) than points with smaller binocular disparities [11, 12]. Therefore, a flat slanted surface has a linear gradient of disparities along the direction of slant [13, 14]. The greater the magnitude of this linear gradient, the greater the perceived slant. Additionally, each eye's image can convey information about slant through texture perspective cues. For example, the retinal projection of texture elements, on average, decreases in size and increases in density as they recede into the distance [15, 16]. The magnitude of these textural gradients is also related to the magnitude of surface slant. Radial distortions introduce non-linear changes in both the binocular and monocular gradients (see Figure 2), which may result in apparent curvature or in other words, changes in slant along a surface. Specifically with pincushion distortion, radially increasing image magnification causes an increase in binocular disparity gradient as well as the texture element spacing toward the periphery (see Fig. 2). Therefore, we predict that the distorted binocular disparity gradient would cause the top portion of a slanted surface (top receding from the observer) to appear more slanted, but the distorted monocular perspective cues would make top portion appear slanted in the opposite direction (toward the observer). The opposite trend would be predicted for the bottom portion of a slanted surface (bottom protruding toward the observer), with slant underestimated based on binocular disparities, but overestimated based on monocular perspective cues. It is difficult to predict how these conflicting binocular and monocular cues will interact and what type of bias in slant perception they will ultimately produce.

In the first of three experiments described here (Experiment 1), textured surfaces were presented in an HMD and observers estimated the slant of a surface at different points in the visual field in two viewing conditions: (1) with uncorrected distortion introduced by HMD lenses and (2) with a standard approach for correction of the lens distortion by barrel distortion pre-warping. Since distortion is stronger toward the periphery, we predicted stronger effects of distortion on slant estimation (systematic misperception of surface slant) in more peripheral relative to central areas. We also predicted that the standard correction model would mitigate these biases.

In Experiment 2, observers adjusted a line (much like in Experiment 1) to match the perceived slant of a surface patch, which had different degrees of slant. In Experiment 3, we tested observers' ability to discriminate the direction of the slant of surface patches relative to a reference surface, both in the presence and absence of simulated lens distortion. With this discrimination paradigm, we were able to estimate the bias and changes in precision due to different levels of pincushion and barrel distortion. Overall, we predicted that the apparent curvature introduced by distortion would make both estimation and discrimination of the average surface slant more uncertain (decreased precision) and resulting in biases (lower accuracy).

The surfaces in Experiments 2 and 3 were presented on a mirror stereoscope, rather than in an HMD, and lens distortion was simulated with a radial distortion model. This provided greater control over viewing conditions and the ability to precisely control the direction and degree of radial distortion. Additionally, our goal was to test the effects of geometric distortion isolated from other possible factors present in HMDs, including but not limited to: chromatic aberration, lens glare, discomfort and lower display resolution. Furthermore, using a small image patch allowed us to get average estimates of surface slant within the central region of the visual field.

2. GENERAL METHODS

2.1 *Image Rendering and Application of Distortion*

Images were rendered and displayed using Matlab's (2018b, MathWorks) Psychtoolbox and OpenGL libraries. We used an off-axis stereo camera model to compute the perspective projection of vertices on a flat 4-m-wide planar surface to the left and right cameras. The center of the surface was placed 15 cm behind the virtual "screen plane", which was set 74 cm from the cameras (matching the stereoscope viewing distance). The lateral offset of the cameras was matched to the inter-pupillary distance (IPD) for each observer, which were measured with a Digital PD meter with 0.5 mm precision (Newtry CP-32BT). Slanted surfaces were modeled

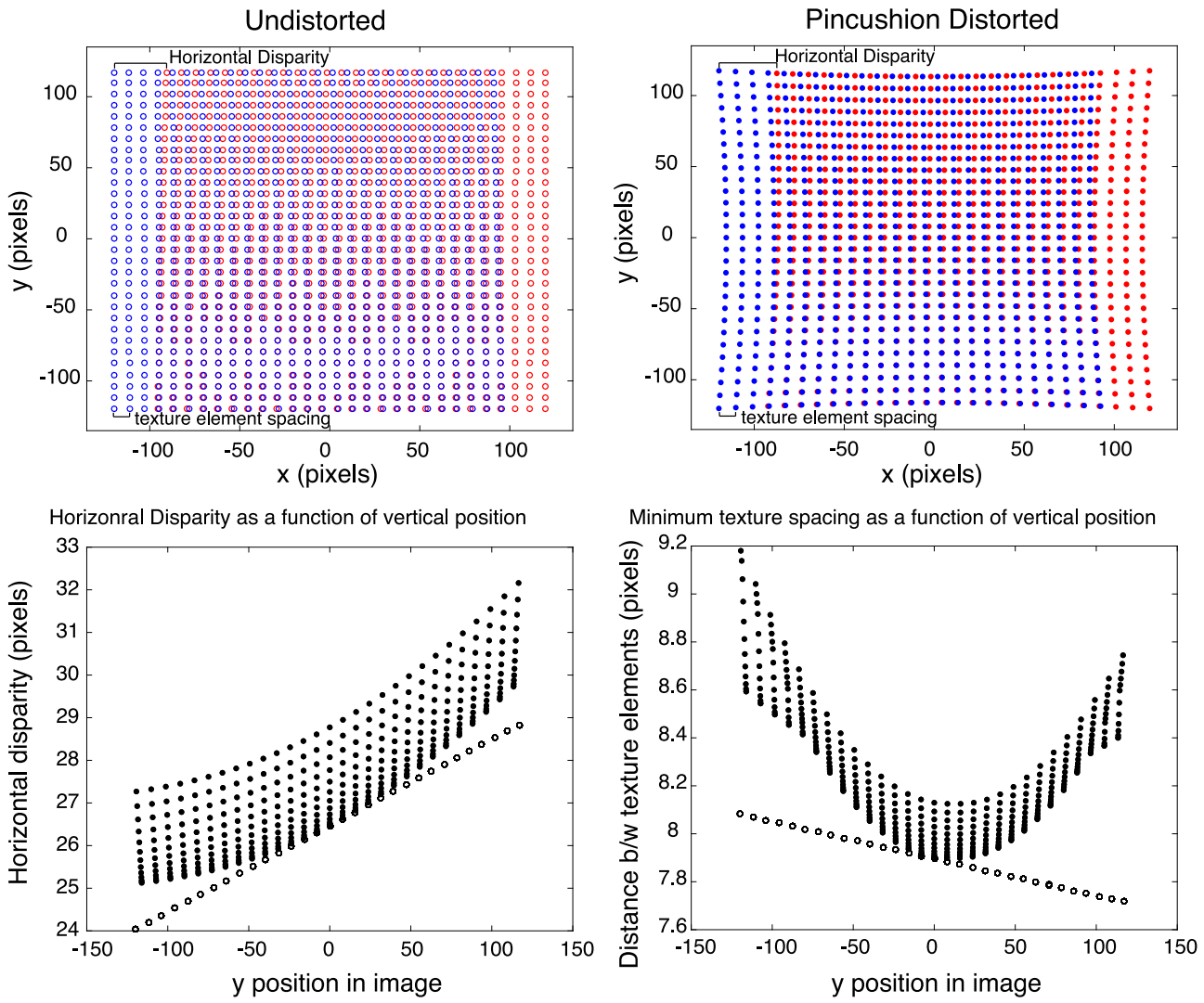

Figure 2. Top panel: Perspective projection of points on a flat surface, placed behind the fixation plane and slanted by 15°, without distortion (top-left, open points) and with distortion (top-right, solid points) for the left (blue) and right (red) eyes. Bottom panel: the derived horizontal disparities from corresponding points in left and right eye projections as a function of the vertical position in the image (left). The derived minimum spacing between points, representing texture spacing, as a function of the vertical position in the image (right). Solid points represent the pincushion distorted case and open points represent the undistorted case.

by rotating the surface plane about a horizontal axis through the surface's center, which was aligned with the midpoint between the two cameras. A set of seven surface slant angles was rendered for each experiment (see Methods for details pertaining to each experiment).

A Voronoi texture (1813 × 1431 pixels), also generated in Matlab, was mapped on to the surface with its position along the surface randomly varied to create 10 texture variations for each slant. The projected images from the left and right camera perspectives were rendered and stored for subsequent distortion transformation and display.

To model lens distortion, each pixel in the image was radially remapped to a new location with the following simplified radial distortion equation:

$$r_d = r + kr^3, \tag{1}$$

where a pixel with a radial distance, r (in pixels), from the image center is remapped to the distorted radial distance, r_d. The coefficient, k, sets the magnitude and direction of distortion. Barrel distortion is the remapping of points toward the image center (negative coefficient), while pincushion distortion is the remapping of points away from the image center (positive coefficient). A coefficient of $k = 1 \times 10^{-6}$ was used, for the inverse of Eq. (1), to correct the HMD distortion in Experiment 1. This correction was determined using a psychophysical nulling procedure by incrementing the coefficient value from 0 to 3×10^{-6} in steps of 0.5×10^{-6} until a regular grid appeared free of curvature (and again in the reverse direction). A similar subjective method was used by Kuhl et al. [7] to correct distortion. We used the average coefficient obtained from both the ascending and descending passes. The final predistortion

amounted to a maximum shift of approximately 22%, relative to the image size (diagonal image radius). Note the similar levels of predistortion used in this headset and in the more widely used Oculus Rift. Coefficients of $k = 1 \times 10^{-6}$ and 3×10^{-6} were used to produce low (≈1%) and high (≈5%) levels of distortion respectively for Experiments 2 and 3. Pixel values in regions neighboring the transformed pixels were bi-linearly interpolated using Matlab's resample function in the image processing toolbox.

3. EXPERIMENT 1: METHODS

3.1 *Participants*

In total, 6 observers were recruited to participate in the experiment (4 females, 2 males, age range: 23–33 years, IPD range: 59–70 mm). All participants had normal or corrected to normal visual acuity and stereoacuity thresholds of at least 40 arcseconds (assessed using the Randot Preschool Stereotest).

3.2 *Head-Mounted Display Setup*

A Google Pixel 2 XL Android device (with native resolution of 2880 × 1440 p at 538 ppi) was connected to a laptop (Alienware model number M17xR4) via a USBC cable and set to mirror the monitor with a resolution of 1920 × 1080 p (using the Splashtop Wired xDisplay app for Android/Windows 64 bit) to which Psychtoolbox drew the pre-rendered images. The Android device was horizontally mounted in a Google Daydream 2 headset (field of view: 100°, IPD: 64 mm) and displayed images stereoscopically to the left and right eyes. Care was taken to center the display in the headset: a line demarcating the center of the display field was placed equidistant between the centers of each optical lens, a point marked by a rubber grip on the headset, during mounting of the device. This permitted precise presentation of stereoscopic image pairs on each half of the screen separately to each eye. Observers rested their chin on a chinrest to minimize head movements. See Figure 3 for a picture of the experimental setup.

3.3 *Procedure*

Observers estimated the local slant of a test surface. On each trial, an image of a textured surface (with slants ranging from 0° to 30° in 5° steps) was stereoscopically presented through the VR headset. The stereo-image pairs (60 × 960 pixels) were presented on the left and right sides of the display; the original surface images were presented on half of the trials (lens distortion, "uncorrected" condition) and on the remainder of the trials, images pre-warped with barrel distortion were presented; we will refer to these trials as the "corrected" condition (see General Methods Section 2.1 for a brief description of how we applied the barrel distortion). A 4-pixel-wide, red probe dot placed in one of six possible screen locations: these locations fell roughly in the top-left, top-right, middle-left, middle-right, bottom-left and bottom-right portions of the display (see Figure 4 for a schematic and probe positions). The observers were instructed to estimate the slant of the surface at the probe position. Since pincushion distortion produces apparent surface curvature (non-uniform slant throughout), observers were asked to imagine a plane tangent to that position on the surface and report its slant if the apparent curvature made it difficult to estimate a single slant. Observers indicated their estimates by adjusting the tilt of a line in the center of the screen, which represents the surface from a side-profile view. To disambiguate the mapping between the orientation of the line and the direction of perceived surface slant, a small arrow representing the observer's vantage point was positioned facing the adjustment line. The line was presented monocularly to the left eye. The probe dot was also presented monocularly either to the left or right eye, depending on whether it fell on the left or right halves of the display, respectively. After each trial, a black screen was displayed for 300 ms followed directly by the next trial. In total, there were 252 trials, 7 slant angles × 2 distortion conditions (corrected and uncorrected) × 3 probe locations (top, middle and bottom) × 6 repetitions per condition. The left versus right position of the probe was determined randomly on each trial, as was the texture variation. The order of presentation of each condition was also randomized. To minimize the effects of chromatic aberration, the images and adjustment line were presented monochromatically using the green channel (see Fig. 4 for example screenshots of the content displayed through the headset on a given trial).

Figure 3. A picture of the setup for Experiment 1. Observers estimated slant by adjusting a line with a knob in their right hand. They registered their response by keyboard press on their left hand. A chinrest stabilized their head.

3.4 *Analysis*

A regression analysis was performed for each observer's mean estimates as a function of the true slant angle. This was performed for each distortion condition and probe location condition. We then submitted the slopes and intercepts to two separate two-way ANOVAs with probe position (top, middle and bottom) and distortion condition (corrected

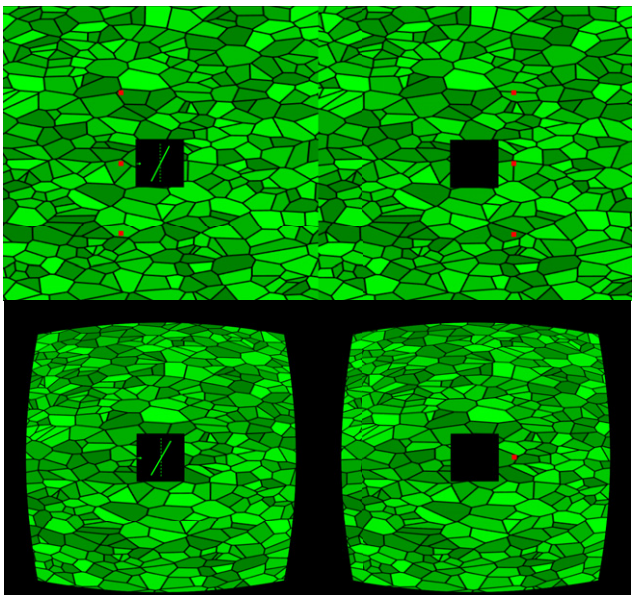

Figure 4. The upper panel shows the stimulus along with the six possible test locations in each eye. The bottom image is a screen shot of a trial (corrected condition, with barrel distortion pre-warping), only one probe is presented and the observer adjusts the measurement line to match perceived slant at the probe. Note: surfaces appear much differently in the HMD with lens distortion.

and uncorrected) as factors. We tested for significant biases in slant perception by carrying out one-sample t-tests on the intercept values, with the null hypothesis that intercepts were 0. Finally, we assessed changes in sensitivity to slant due to distortion by carrying out paired t-tests comparing regression slopes across distortion conditions. All significance levels were subject to Holm–Bonferroni correction.

4. EXPERIMENT 1: RESULTS

To probe the effect of distortion on local slant estimates as a function of slant angle, linear regressions were carried out for each observer in each condition. R-square values for the uncorrected conditions were, on average, quite low (mean = 0.497, SD = 0.36), likely reflecting ceiling and floor effects of slant estimates across slant angles; observers consistently reported high slants when the probe was in the bottom portion of the display and they consistently reported low slants when the probe was in the top portion of the display. In contrast, R-square values were quite high, on average, in the corrected conditions (mean = 0.797, SD = 0.19) reflecting the ability of observers to better track changes in local surface slant when distortion correction was applied. This was further validated by a two-way ANOVA on regression slopes with probe position (top, middle and bottom) and distortion condition (corrected and uncorrected) as factors: there was a significant effect of probe position ($F_{2,10} = 6.44, p = 0.0159, \eta_p^2 = 0.56$) and distortion condition ($F_{1,5} = 19.98$, $p = 0.0066$, $\eta_p^2 = 0.80$) on the slopes of the regression lines. No significant interaction between probe position and distortion correction was found

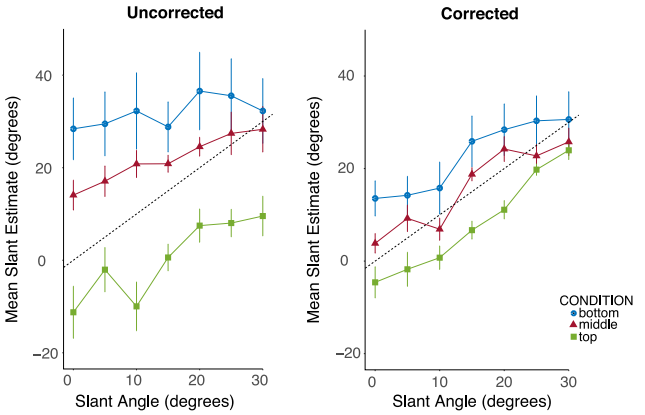

Figure 5. Mean slant estimates across observers (error bars represent ±SEM) for each surface slant at different probe locations (colors) in Experiment 1. Left and right panels show results for uncorrected and corrected distortion conditions, respectively.

Table I. A summary of t-test results comparing regression intercepts against zero. Shaded entries refer to statistical significance after Holm–Bonferroni correction.

Condition	Intercept ≠ 0
Uncorrected, Top	$t_5 = -2.52, p = 0.053$
Uncorrected, Middle	$t_5 = 5.576, p = 0.00255$
Uncorrected, Bottom	$t_5 = 4.266, p = 0.00797$
Corrected, Top	$t_5 = -2.005, p = 0.1013$
Corrected, Middle	$t_5 = 1.9245, p = 0.1123$
Corrected, Bottom	$t_5 = 2.94, p = 0.0323$

($F_{2,10} = 1.62$, $p = 0.246$, $\eta_p^2 = 0.24$). Overall, the slopes in the corrected conditions were greater than those in the uncorrected conditions, suggesting decreased sensitivity to changes in local surface slant in the presence of high distortion (see Figure 5).

An ANOVA on regression intercepts with probe position (top, middle and bottom) and distortion condition (corrected and uncorrected) as factors revealed significant effects of probe position ($F_{2,10} = 15.99, p = 7.6 \times 10^{-4}, \eta_p^2 = 0.76$) and distortion ($F_{1,5} = 10.71$, $p = 0.022$, $\eta_p^2 = 0.68$). A significant interaction between probe position and distortion correction was found ($F_{2,10} = 10.60, p = 0.003, \eta_p^2 = 0.68$).

One-sample t-tests on the intercept values, against a null value of zero, revealed significant biases for the uncorrected/middle probe condition ($t_5 = 5.58, p = 0.00255$) and the uncorrected/bottom probe condition ($t_5 = 4.26$, $p = 0.00797$). All other conditions were not significant according to the Bonferroni adjusted $\alpha = 0.0083$ (see Table I for full statistics and Figure 6 for the plot).

Paired t-tests comparing regression slopes across distortion conditions revealed significant differences between corrected and uncorrected middle probe conditions ($t_5 = -3.94$, $p = 0.011$) and corrected and uncorrected bottom probe conditions ($t_5 = -4.411$, $p = 0.007$) (see Figure 7). When the probe was in the top of the display, there was

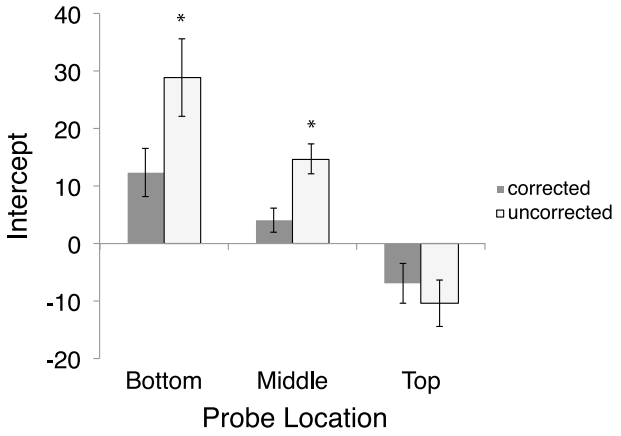

Figure 6. Mean regression intercepts across observers in Experiment 1. Asterisk represents significant differences from zero. Error bars represent ±SEM.

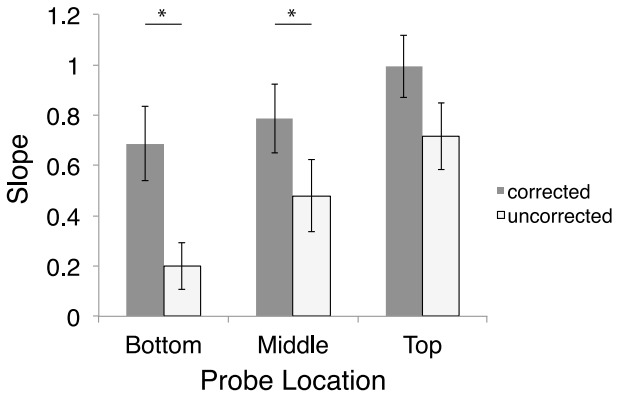

Figure 7. Mean regression slopes across observers in Experiment 1. Asterisk represents significant differences. Error bars represent ±SEM.

no significant difference between corrected and uncorrected ($t_5 = -2.174$, $p = 0.082$).

5. EXPERIMENT 2

In Experiment 1, we found strong biases in local surface slant estimation in the presence of the lens distortion in a head-mounted display. Applying the appropriate level of inverse distortion, determined by eye, greatly reduced the effects of distortion on local slant estimates, but biases remained. In a pair of follow-up experiments we assessed the effects of lens distortion on slant perception, as well as the effects of undercorrecting or overcorrecting the distortion by applying different levels of pincushion and barrel distortion. This necessitated precise control over the level of distortion applied to images of slanted surfaces, and scaling of the image so that it was limited to the central portion of the visual field. Therefore, Experiments 2 and 3 were conducted using a mirror stereoscope display with image transformations (see Section 2.1 and Eq. (1)) introduced to achieve the desired levels of distortion.

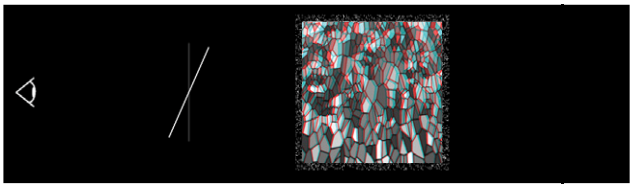

Figure 8. Surface slant estimation task (schematic of a typical trial). The surface is shown here in red-cyan for color anaglyph viewing (in digital version only).

5.1 *Experiment 2 Methods*

5.2 *Participants*

We recruited 11 observers to participate in the experiment (8 females, 3 males, age range: 20–36 years). Of these observers, 5 participated in Experiment 1.

5.3 *Stereoscope Setup and Stimulus Display*

Computer generated images of slanted surfaces were displayed using a Wheatstone mirror stereoscope, which independently displayed left and right stereo-image pairs on Dell LCD monitors (model number: U2412Mb; dimensions: 52 × 32 cm; refresh rate: 60 Hz) to the left and right eyes. The peak luminance of each monitor was 148 cd/m^2 (through the stereoscope mirror: 97.53 cd/m^2). Each monitor had a resolution of 1920 × 1200 pixels with a density of 48 pixels per degree at a viewing distance of 74 cm so each pixel subtended 1.25 arcmin.

The surfaces (grayscale images) were presented behind a 5° square aperture. A frame with a width of 0.3° defined the aperture, and was textured with a random dot pattern (see Fig. 4). The frame served as a fusion guide and was randomly displaced in depth by −0.04°, 0° or 0.04° to make the distance between it and any point on the surface uninformative for slant estimation.

5.4 *Procedure*

Trials started with a central fixation cross that appeared for 750 ms. Immediately following this, the surface, aperture and reference frame appeared in the center of the screen. The icon for slant matching task was presented simultaneously to the left of the test stimulus. As in Experiment 1, an icon (in this case an eye symbol) disambiguated the perspective of the observer relative to the surface represented by a line. Observers adjusted the rotation of the line (1° of precision) with a rotary encoder knob. A dark-gray reference line representing frontoparallel (0° slant) was displayed with the white adjustment line. The surface remained displayed until the observer registered their response with a key press. See Figure 8 for a schematic of the display for Experiment 2.

Surface slants ranged from 0° to 30° in steps of 5°. The surfaces were either non-distorted (ND), or distorted with 5% barrel distortion (BD) or pincushion distortion (PD). Each combination of surface slant and distortion condition was presented 15 times for a total of 315 trials per test session (15 repetitions × 7 slants × 3 Distortion conditions). The presentation order of trials was randomized. Observers were given a break midway through the 30 min session.

Table II. A summary of t-test (one-tailed) results comparing mean estimates of ND to distortion conditions. Shaded entries indicate statistical significance after Holm–Bonferroni correction.

Angle	ND > BD	ND > PD
0°	$t_{10} = -1.57, p = 0.92$	$t_{10} = -2.43, p = 0.98$
5°	$t_{10} = -0.22, p = 0.58$	$t_{10} = -0.38, p = 0.64$
10°	$t_{10} = 1.20, p = 0.13$	$t_{10} = 1.63, p = 0.067$
15°	$t_{10} = 3.13, p = 0.0053$	$t_{10} = 3.16, p = 0.0050$
20°	$t_{10} = 2.11, p = 0.030$	$t_{10} = 3.72, p = 0.002$
25°	$t_{10} = 2.77, p = 0.01$	$t_{10} = 4.28, p = 0.0008$
30°	$t_{10} = 3.02, p = 0.0064$	$t_{10} = 4.61, p = 0.0005$

5.5 *Analysis*

We computed the mean slant estimate for each condition for each observer. Difference scores, for each condition, were calculated by subtracting the mean slant estimate by the true slant angle. One-sample t-tests (one-tailed) were done, for each distortion condition, on the mean difference scores averaged across slant angles. The null hypothesis was that mean difference scores were not significantly different from zero. The alternative hypothesis was that difference scores were significantly less than zero (underestimation of slant). P-values were Bonferroni adjusted to control for the family-wise error rate.

A two-way repeated-measures ANOVA was performed on the mean estimate values, with slant angle and distortion condition as factors. Given a significant effect of distortion condition, we carried out pair-wise t-tests (one-tailed) comparing mean slant estimate for ND against PD and ND against BD conditions at each slant angle. Since a total of 14 comparisons were done, p-values were adjusted using the Holm–Bonferroni method to control for the family-wise error rate.

A regression analysis was performed for each observer's mean estimates as a function of the true slant angle. This was performed for each distortion condition. We then compared the slopes from the regression analysis of ND against PD and ND against BD conditions (pair-wise one-tailed t-tests). P-values were Bonferroni adjusted to control for the family-wise error rate.

6. EXPERIMENT 2: RESULTS

We tested the hypothesis that slant angle would be underestimated in the distortion conditions (BD, PD and ND) and found a significant underestimation of mean estimates in the BD condition ($t_{10} = -4.3$, $p = 0.00078$) and in the PD condition ($t_{10} = -3.79$, $p = 0.0017$). There was no significant underestimation of slant angle for the ND condition ($t_{10} = -1.97$, $p = 0.038$) after adjusting the alpha level to control for family-wise error rates ($\alpha = 0.0167$).

Observers' mean estimates of slant angle, as a function of true slant angle, followed a linear trend. The mean R-square value for linear regressions was 0.937 (SD = 0.046). The two-way repeated-measures ANOVA on mean slant estimates revealed significant effects of slant angle ($F_{1,10} = 146.56$, $p = 2.6 \times 10^{-7}$, $\eta_p^2 = 0.93$) and distortion type ($F_{2,20} = 4.9$, $p = 0.018$, $\eta_p^2 = 0.32$) and a significant interaction between slant angle and distortion type ($F_{2,20} = 24.81$, $p = 3.8 \times 10^{-6}$, $\eta_p^2 = 0.71$).

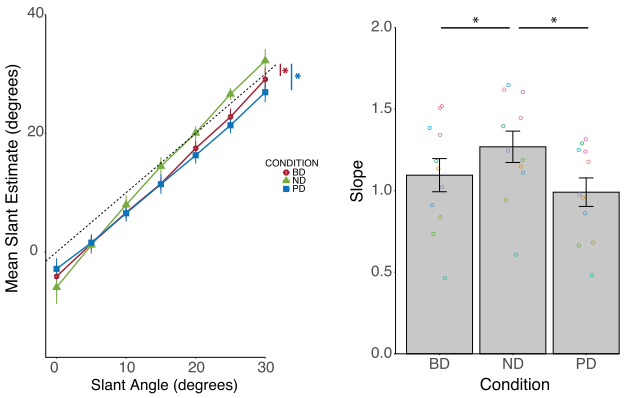

Figure 9. A: Mean slant estimation for barrel (circles), pincushion (squares) and no (triangles) distortion in Experiment 2. Asterisks indicate a significant difference from ideal performance B: Slopes of individual observer regression fits for the three conditions; points represent individual observer values (color-coded). Asterisks indicate pair-wise comparisons with significant differences.

Paired t-tests revealed significant underestimation of slant in the PD condition, relative to the ND condition, for three out of seven tested angles (20°, 25° and 30°). See Table II for a full summary of paired t-test results.

Therefore, slant estimates were underestimated for both distortion conditions (BD and PD) relative to ideal performance. However, relative to the ND condition (distortion-free), only the pincushion distortion showed underestimations for a number of tested angles (see Figure 9a).

Paired t-tests revealed that slopes obtained from regressions on both the BD and PD estimates were significantly shallower than the slopes obtained for the ND condition (BD < ND: $t_{10} = 4.15$, $p = 0.001$; PD < ND: $t_{10} = 7.11$, $p = 3.2 \times 10^{-5}$; $\alpha = 0.025$). Therefore, sensitivity to changes in slant is lower in the presence of either type of distortion (PD & BD) compared to ND (see Fig. 9b).

7. EXPERIMENT 3

In Experiment 2 we measured the estimation of average surface slant in the presence of 5% barrel and pincushion distortion, as well as without distortion. We found that pincushion distortion, and to a lesser extent barrel distortion, caused an underestimation of average surface slant. In Experiment 3 we assessed the effects of high (5%) and low (1%) levels of barrel and pincushion distortion on the discrimination of surface slants. Once again, we used the stereoscope setup described in Experiment 2 to precisely display stereoscopic images with simulated distortion.

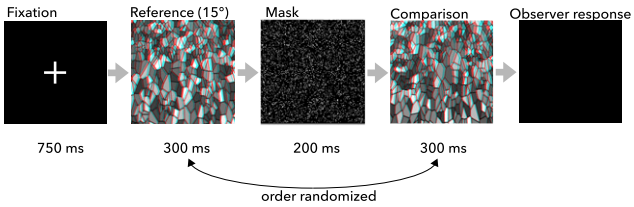

Figure 10. Surface slant discrimination task. Observer indicates which surface appears to have the greater slant. Surfaces are shown here in red-cyan for color anaglyph viewing (in digital version only), but were presented in full color in the experiment.

7.1 *Experiment 3 Methods*

7.2 *Participants*

In total, 11 observers were recruited to participate in the experiment (8 females, 3 males, age range: 20–31 years, IPD range: 60–72 mm). All participants had normal or corrected to normal visual acuity and stereoacuity thresholds of at least 40 arcseconds (assessed using the Randot Preschool Stereotest). One observer's data was excluded from analysis due to poor performance on the baseline (distortion-free condition; see section 7.3 Procedure for more details).

7.3 *Procedure*

We tested observers' ability to discriminate the direction of slant of surfaces (distorted or undistorted) relative to a distortion-free reference surface with a 15° slant. As shown schematically in Figure 10, each trial started with a central fixation cross that appeared for 750 ms, followed immediately by the first stimulus (either the reference surface or one of the comparison surfaces) for 300 ms. A random element mask was shown for 200 ms and the second surface was then presented for 300 ms.

Comparison surfaces were either non-distorted (ND), or distorted with a low level (1%) or a high level (5%) of barrel distortion (BD) or pincushion distortion (PD) for a total of 5 distortion conditions.

Observers were instructed to indicate, by button press on a gamepad, which surface (first or second) appeared more slanted. No feedback was given. The 40 min experiment was divided into 2 blocks. Each block contained 525 trials: 5 distortion conditions × 7 comparison slants × 15 repetitions. The order of presentation of all trials was randomized. Observers were given breaks after half of the trials in a block.

In the first block, comparison surfaces had slants of 7.5° –22.5° in steps of 2.5°. After the first block, performance in the ND condition was assessed to meet the following criterion: the observer should be able to reliably detect (75% of the time) that the lowest tested comparison slant is less slanted than the reference, and that the highest tested comparison slant is more slanted than the reference; the experiment was concluded if the criterion was still met after the 2 blocks. Otherwise, the first block was disregarded and the full experiment was run with an extended range of 0° to 30° in 5° steps. If the observer's performance, in the ND condition, still did not meet the criterion, their data were excluded. In either range of tested slants, the median value was 15° (same as the reference) to ensure equal sampling on either side of the reference slant.

7.4 *Analysis*

For each observer, the proportion of times the comparison was judged to be more slanted at each tested surface slant was computed and fit with a cumulative normal function [17]. The μ and σ parameters of the best-fit (maximum likelihood) cumulative normal function were used for further analysis. The μ parameter corresponds to the comparison slant that would be judged as more slanted than the reference 50% of the time; this is also known as the point of subjective equality (PSE). The difference in comparison slant between the PSE and the point at which the comparison slant is reliably judged as more slanted than the reference (at a rate of 75%) is taken to be the just-noticeable difference (JND).

The PSE for each distortion condition was further analyzed to test for significant biases (shifts in PSE) in the distortion conditions relative to the ND condition. A repeated-measures ANOVA was performed on the PSE values (dependent variable) extracted for each subject, with distortion condition (five levels) as the factor. Given a significant effect of distortion condition, we did planned comparisons (t-tests) to assess which distortion conditions, BD and PD, had significantly different PSEs from the ND condition. The significance level was Bonferroni adjusted to control for the family-wise error rate ($\alpha = 0.0125$).

The JND for each distortion condition was further analyzed to test for significant changes in precision in the distortion conditions relative to the ND condition. A repeated-measures ANOVA and subsequent planned comparisons were performed on the JND values in the same manner described above.

8. EXPERIMENT 3: RESULTS

Observer performance on the discrimination task was well fit by cumulative normal functions (see Figure 11). The repeated-measures ANOVA with PSE values as the dependent variable and distortion condition as a factor revealed a significant effect of distortion condition ($F_{4,36} = 4.11$, $p = 0.0076$ (Huyn–Feldt corrected), $\varepsilon = 1.03$, $\eta_p^2 = 0.31$).

Planned comparisons revealed significantly greater PSEs for the high (5%) PD condition compared to the ND condition ($p < 0.05$). However, planned comparisons for the low distortion (1%) conditions did not reveal any significant differences (see Table III for a summary of t-test results). Therefore, only the 5% pincushion distortion resulted in a significant bias (underestimation) in perceived slant relative to non-distorted surfaces (see Figure 12a).

The repeated-measures ANOVA with JND values as the dependent variable and distortion condition as a factor revealed a significant effect of distortion condition ($F_{4,36} = 11.68$, $p = 3.5 \times 10^{-6}$ (Huyn–Feldt corrected), $\varepsilon = 0.47$, $\eta_p^2 = 0.56$).

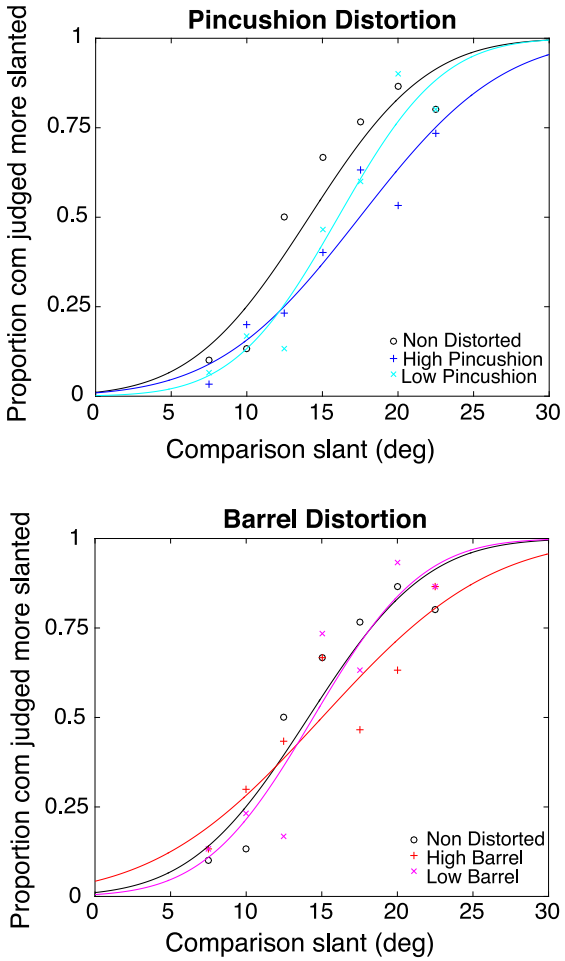

Figure 11. Performance of a representative observer on the discrimination task (Experiment 1). Solid curves represent best-fit psychometric functions.

Table III. A summary of pair-wise *t*-test results comparing the PSEs of distortion conditions against the distortion-free condition. Shaded entries represent statistical significance.

PSEs, $\alpha = 0.0125$	BD high > ND	BD low > ND	PD high > ND	PD low > ND
t_9	−1.49	−2.24	−3.96	−1.91
p	0.17	0.052	0.0033	0.088

Planned comparisons revealed significantly greater JNDs for the high (5%) PD condition compared to the ND condition ($p < 0.05$) and the 5% BD condition compared to the ND condition ($p < 0.05$). All remaining planned comparisons were not significantly different (see Table IV for a summary of *t*-test results). Therefore, relative to distortion-free surfaces, high levels of both pincushion and barrel distortion resulted in a significant decrease in precision (increase in JND) in perceived slant (see Fig. 12b).

8.1 *Discussion*

We have shown that the uncorrected lens distortion in a representative HMD greatly biases the estimation of

Table IV. A summary of *t*-test results comparing the JNDs of distortion conditions against the distortion-free condition. Shaded entries represent statistical significance.

JNDs, $\alpha = 0.0125$	BD high > ND	BD low > ND	PD high > ND	PD low > ND
t_9	−3.84	−2.25	−4.56	−2.48
p	0.004	0.051	0.0014	0.035

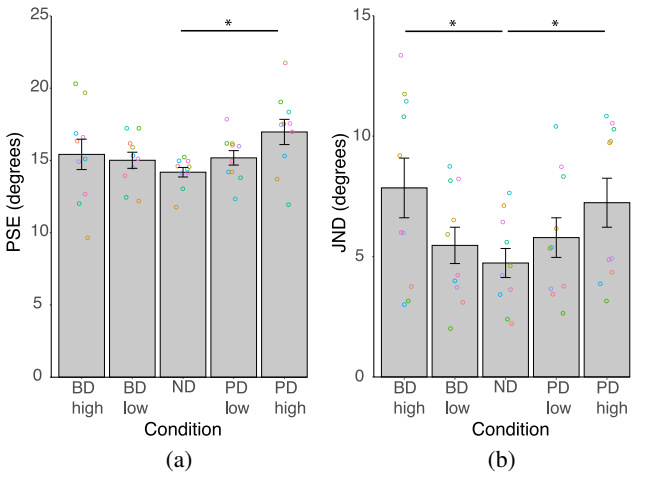

Figure 12. A: Point of subjective equality (PSE). B: Just-noticeable difference (JND). Points represent individual observer data (color-coded) for each of the test conditions (barrel distortion = BD; pincushion distortion = PD; no distortion = ND). The bar plots represent the means (error bars represent ±SEM). Asterisks represent comparisons that had significant differences.

local surface slant. Specifically, surface slant near the top of the display tends to be underestimated while surface slant near the bottom, or near the middle, of the display tends to be overestimated. Furthermore, conventional means of correcting this distortion greatly reduced, but did not eliminate, the bias in local surface slant estimation.

As outlined in the Introduction, the pincushion distortion applied in Experiment 1 introduced opposite patterns of perceptual distortions for monocular texture gradients compared with binocular disparity. That is, after distortion is applied, texture elements systematically become larger toward the periphery. This texture pattern is consistent with a concave surface (middle receding away from the observer), which would cause the top portion to appear to slant toward the observer (underestimation) and enhanced slant in the bottom region (overestimation). The binocular disparity gradients are warped in the opposite direction, and so predict the appearance of a convex surface. It is clear from our results that the 2D texture gradient dominated perceived slant in our stimuli. This is interesting, particularly given that the Voronoi texture was chosen because it would minimize texture-based depth information such as perspective foreshortening. While the binocular disparities generated by our slanted surfaces were typically well above threshold, other factors may have served to make them less reliable than the monocular depth information. For instance,

monocular regions are created by the HMD nose cutout that are framed by the binocularly visible headset contours. Further, in addition to magnifying horizontal binocular disparities, pincushion distortion introduces small vertical disparities in the periphery. The variation in these vertical offsets in the periphery may have added uncertainty to judgments of slant about the horizontal axis. Additional studies are needed to evaluate the relative impact of monocular and binocular cues in the presence of such distortions.

These biases were still apparent, and in the same direction, even after we corrected for barrel distortion. In our study the correction was determined psychophysically by a single observer using a nulling procedure. It is clear that residual pincushion distortion was present. While the lens distortion may have been eliminated for one observer, individual anatomical and visual sensitivity differences will result in greater or less required distortion correction, and therefore differences in perceived residual distortion. These results suggest that sophisticated approaches to modeling lens distortions are needed, perhaps even on an observer-by-observer basis. It should be noted that applications designed for consumer HMDs have built-in distortion correction, which is not customized for individual observers. The presence of similar slant distortions can be confirmed by simply viewing frontal surfaces generated in a given application and viewed through the HMD.

The large and consistent local distortions recorded in Experiment 1 produce an overall perception of surface curvature. In Experiments 2 and 3 we evaluated the extent to which the perceived average slant across the surface was influenced by radial distortions. We examined the effects of distortion on the estimation of average slant (Experiment 2) and the discrimination of average slant near threshold (Experiment 3). To investigate the consequences and sensitivity to this residual distortion under more controlled conditions, we measured the effects of distortion on slant bias relative to a frontal plane in Experiment 2, and relative to an undistorted surface in Experiment 3. In these experiments we looked at the effects on average slant for surfaces presented in the center of the field of view. While geometry predicts effects should be reduced in the center of the display, Experiment 2 found there were still significant distortions in this region. Together, these experiments, showed slant discrimination is degraded by radial distortions at or above 5%. Furthermore, at this level of distortion there are significant biases in slant perception such that distorted surfaces appear less slanted than distortion-free surfaces. While effects at 1% distortion were roughly proportional to those at 5% levels, they were not large enough to introduce statistically measurable effects on bias or precision compared to no distortion. Thus we expected small amounts of residual distortion (less than or equal to 1%) to have minimal effects on slant perception at or above threshold.

Interestingly, there is an asymmetry between the two distortion types, with a stronger bias toward frontoparallel (0° slant) for pincushion distortion. Given this asymmetry, it is crucial to sufficiently correct the initial distortion caused by optical lenses, often pincushion type. Our results suggest that overcorrection of the initial distortion, and incurring residual amounts of barrel distortion, will have fewer perceptual consequences than undercorrection. The levels of distortion we tested (1% and 5% for both types) could be interpreted as reasonable levels of residual distortion resulting from under or overcorrecting a baseline pincushion distortion of 10%, as measured by Kuhl et al. [7]. However, as mentioned above, the level of baseline distortion is likely to vary considerably across consumer HMDs. The baseline distortion tends to be considerable in modern consumer HMDs that rely on distortion correction through image processing rather than optical design to reduce size, weight and cost.

8.2 *Relation to Previous Work*

In Kuhl et al.'s [7] study, a level of 10% pincushion distortion failed to produce any significant effects on distance estimation through blind walking. Their target distances from observers ranged from 3 to 6 m, and the ground inclination in their virtual environments were far from frontoparallel. In contrast, our surfaces appeared no farther than a meter from observers, and surface inclinations deviated no more than 30° from frontoparallel. Furthermore, our task required the use of disparity and texture gradients across the surface, rather than estimates of depth at single locations. Therefore, radial distortions may differentially effect distance estimation of far and near surfaces as well as for estimations of depth gradients versus absolute depth estimates.

Slant underestimation is a common occurrence in the absence of precise cues to depth [18–20]. The relationship between low precision and enhanced bias is often described with Bayesian cue combination models: slant estimation can be modeled as a weighted average between different depth cues and an assumed prior for zero slant (frontoparallel) [21, 22]. When depth cues are imprecise they are given lower weighting relative to the prior, which "pulls" the estimate toward frontoparallel [18].

The existence of a frontoparallel prior alone cannot explain the asymmetry we have measured in the biases produced by different distortions. Given that our manipulation is a systematic modulation of depth cues, rather than the simple addition of depth noise, we must consider the possibility that distortion may have direct biasing effects on disparity and texture gradients. The opposite signs of curvature in pincushion and barrel distortions may be the basis of the asymmetry in the frontoparallel bias (Fig. 2). Furthermore, we note that for surfaces falling behind the screen plane (as in Experiments 1 and 2), radial distortions introduce a cue conflict between monocular texture and binocular disparity cues: these depth cues will have opposite signs in their apparent curvature. This cue conflict is another potential source of bias and/or decreased precision. Future work will attempt to identify the contributions of each cue's warping effects in producing the overall bias.

9. CONCLUSION

When viewing surfaces in an HMD, without distortion correction applied, local slant estimation is significantly biased in a manner consistent with the warping of texture-based monocular cues. Even with distortion correction applied, residual levels of distortion caused biases in local slant estimation. Using a mirror stereoscope we have shown that 5% distortion has measurable negative impacts on the precision and accuracy of average slant perception; however, at 1% distortion these effects were not measurable. Furthermore, different types of distortion have differential effects: pincushion distortion has a greater impact overall on depth perception. With these insights in mind, developers of HMDs or VR related content might better anticipate and counteract the effects of optical distortion to improve the viewer experience. Particularly, our results show how the failure to adequately correct for lens distortion has consequences for human perception, and presumably action, in virtual environments. For tasks that require high accuracy and precision in estimating surface shape and orientation, e.g. walking on uneven terrain or placing objects on surfaces, it is especially important to adequately correct lens distortion.

ACKNOWLEDGMENTS

This work was funded by an NSERC Collaborative Research & Development (CRD) grant, in partnership with Qualcomm Canada Inc., and the Canada First Research Excellence Fund (CFREF) for the Vision: Science to Application (VISTA) program.

REFERENCES

[1] J. P. Wann, S. Rushton, and M. Mon-Williams, Vis. Res. **35**, 2731 (1995).
[2] E. Hecht, *Optics*, 3rd edn. (Addison-Wesley, 1998).
[3] W. Robinett and J. P. Rolland, Presence: Teleoperators and Virtual Environments **1**, 45 (1992).
[4] D. Pohl, G. Johnson, and T. Bolkart, *Proc. 19th ACM Symposium on Virtual Reality Software and Technology* (ACM, New York, NY, USA, 2013), pp. 259–262.
[5] J. P. Rolland and T. Hopkins, *A Method of Computational Correction for Optical Distortion in Head-Mounted Displays* (University of North Carolina at Chapel Hill, Department of Computer Science, 1993).
[6] P. Drap and J. Lefèvre, Sensors **16**, 807–824 (2016).
[7] S. A. Kuhl, W. B. Thompson, and S. H. Creem-Regehr, ACM Trans. Appl. Percept. **6**, 1–24 (2009).
[8] R. S. Allison, I. P. Howard, B. J. Rogers, and H. Bridge, Perception **27**, 1287–1304 (1998).
[9] R. S. Allison and I. P. Howard, Vis. Res. **40**, 1869–1886 (2000).
[10] J. M. Hillis, S. J. Watt, M. S. Landy, and M. S. Banks, J. Vis. **4**, 967–992 (2004).
[11] C. Wheatstone, Phil. Trans. R. Soc. **128**, 371–394 (1838).
[12] I. P. Howard and B. J. Rogers, *Perceiving in Depth* (Oxford University Press, New York, 2012).
[13] M. S. Banks, I. T. C. Hooge, and B. T. Backus, J. Vis. **1**, 55 (2001).
[14] G. J. Mitchison and S. P. Mckee, Vis. Res. **30**, 1781 (1990).
[15] J. J. Gibson, *The Perception of the Visual World* (Houghton Mifflin, Oxford, England, 1950).
[16] D. C. Knill, Vis. Res. **38**, 1655 (1998).
[17] F. A. Wichmann and N. J. Hill, Perception & Psychophysics **63**, 1293 (2001).
[18] J. A. Saunders and Z. Chen, J. Vis. **15**, 14 (2015).
[19] J. A. Perrone, Perception **11**, 641 (1982).
[20] H. Ji and C. Fermüller, Vis. Res. **46**, 3105 (2006).
[21] A. L. Yuille, D. Geiger, and H. H. Bülthoff, Netw., Comput. Neural Syst. **2**, 423 (1991).
[22] B. N. S. Vlaskamp, P. Guan, and M. S. Banks, Front. Psychol. **4** (2013).